tvst

Article

Effect of Vitamin D3 on Regulating Human Tenon's Fibroblasts Activity

Shuo Jia[1], Fushun Chen[1], Huogang Wang[1], Gandhervin Kesavamoorthy[1], Jimmy Shiu-Ming Lai[1], Ian Yat-Hing Wong[1], Kin Chiu[1], and Jonathan Cheuk-Hung Chan[1]

[1] Department of Ophthalmology, LKS Faculty of Medicine, University of Hong Kong, Hong Kong

Correspondence: Jonathan Cheuk-Hung Chan, Department of Ophthalmology, LKS Faculty of Medicine, University of Hong Kong, Room 301, Block B, Cyberport 4, 100 Cyberport Road, Hong Kong.
e-mails: jonochan@hku.hk, jonnochan@yahoo.com

Received: February 12, 2021
Accepted: May 16, 2021
Published: July 12, 2021

Keywords: calcitriol; glaucoma; human Tenon's fibroblasts (HTF); pterygium; RNA sequencing; vitamin D3

Citation: Jia S, Chen F, Wang H, Kesavamoorthy G, Lai JSM, Wong IYH, Chiu K, Chan JCH. Effect of vitamin D3 on regulating human Tenon's fibroblasts activity. Transl Vis Sci Technol. 2021;10(8):7, https://doi.org/10.1167/tvst.10.8.7

Purpose: To study the in vitro effect of vitamin D3 on the healing response of human Tenon's fibroblasts (HTF) and its possible role in preventing excessive postoperative subconjunctival fibrosis.

Methods: Effect of vitamin D3 on cytotoxicity and cell survival of primary cultured HTF was measured by lactate dehydrogenase and PrestoBlue assays, respectively. Proliferation and migration of vitamin D3–treated HTF (D3-HTF) was determined by CyQUANT proliferation and scratch assay, respectively. The mRNA expression profiles of control-HTF and D3-HTF from six subjects (three with glaucoma and long-term use of topical medications, three with primary pterygium) were assessed by RNA sequencing analyses to identify potential biomarkers for the inhibitory effect on HTF by vitamin D3. Validation of these biomarkers and their potential pathways were performed by quantitative real-time polymerase chain reaction (qRT-PCR) detection.

Results: Pure monolayers of HTF from controls (retinal detachment or squint surgeries), pterygium, and glaucoma subjects were successfully prepared and passaged. Proliferation and migration of pterygium and glaucoma HTF were inhibited by vitamin D3 in a dose-dependent manner, and without cytotoxicity or decrease in cellular viability with concentrations up to 10 µM. The qRT-PCR results were consistent with the transcriptome analyses, vitamin D3 appears to enhance CYP24A1, SHE, KRT16 but suppresses CILP expression in HTF.

Conclusions: Vitamin D3 can inhibit the in vitro activity of HTF without compromising cellular survivability at concentration up to 10 µM. This has potential clinical application for improving the outcome of pterygium and filtering surgeries.

Translational Relevance: Vitamin D3 can suppress the in vitro proliferation, migration, and transdifferentiation of human Tenon's fibroblasts, without the cytotoxicity of mitomycin-C, the current standard antifibrotic agent in clinical use.

Introduction

Glaucoma is one of the leading causes for irreversible blindness,[1] characterized by progressive damage to the optic nerve from an intraocular pressure (IOP) higher than its normal tolerance level.[2] Although the tolerance level varies among individuals and the stage of disease, the aim in all cases is reduction of IOP or preventing its elevation.[3] Lowering IOP by medications (usually as eye drops) is the first line of treatment in most clinical practices.[4] When glaucoma progresses because the IOP remains high despite multiple medications, procedures involving lasers or incisional surgeries are often required to prevent blindness.[5] Surgical procedures lower IOP by facilitating aqueous humor to exit the eye by decreasing the outflow resistance.[6] Currently, the most common methods of lowering outflow resistance is by diverting aqueous out of the anterior chamber and into the subconjunctival space. Access to the

subconjunctival space is by either surgically creating a new opening or inserting a stent-type implant into the anterior chamber.[7] However, conjunctival wound healing after such drainage surgeries can sometimes be excessive, leading to subconjunctival fibrosis and scarring at the drainage site, with progressive reduction of aqueous outflow and surgical failure.[8] Aside from surgery, long-term use of topical glaucoma medication can also activate human Tenon's fibroblasts (HTF).[9] Excessive activation of HTF result in their proliferation and migration, synthesis of extracellular matrix components (ECM), and collagen contraction, leading to subconjunctival scarring.[10] Various methods have been used for modulating postoperative wound scarring, but one that is free from serious adverse effect remains an elusive goal for subconjunctival aqueous drainage procedures.[11]

Aside from its role in postoperative scarring after glaucoma surgery, HTF is also involved in the development of pterygium. Although pterygium excision is a relatively simple procedure, recurrences are common and more difficult to excise than primary pterygium in the initial surgery,[12] so measures to mitigate proliferation of HTF after surgery are used to decrease the incidence of recurrent pterygium.[13]

Antimetabolites such as 5-fluorouracil (5-FU) and mitomycin-C (MMC) are commonly used as antifibrotic agents to prevent or reduce postoperative fibrosis and scarring,[14] but their use is limited by the cellular toxicity common to most antimetabolites, which manifests clinically as impaired wound healing and atrophic conjunctiva at the drainage site, with increased risk of bleb leak, hypotony, exposed implant, and infection.[15] Therefore any new agents that can suppress fibrosis and scarring without concomitant cellular toxicity will greatly improve glaucoma surgery outcome.[16]

Vitamin D3 (abbreviated as D3) is a multifunctional hormone that not only affects calcium homeostasis but plays an essential role in immune system regulation, as well as cell growth and survival.[17] Many tissues in the eye are able to both activate and respond to D3,[18] whereas D3 levels and genetic variations can influence the development of a wide range of ocular pathologies, such as myopia, age-related macular degeneration, diabetic retinopathy, uveitis, and glaucoma.[18] Previous studies have shown that D3 may play a protective role in ocular health.[19] This included inhibition of angiogenesis in transgenic murine retinoblastoma,[20] inhibition of corneal neovascularization induced by sutures in murine eyes,[21] inhibition of retinal neovascularization in mice model,[22] prevention of retinal autoimmune disease and mitigation of uveitis,[23] decreased retinal inflammation and levels of amyloid beta (Aβ) accumulation,[24] as well as lower IOP in primates.[25]

Because D3 appears to have a modulating effect on cutaneous scar formation,[26] it may be potentially useful in ocular surgeries, although whether conjunctiva or Tenon tissues will respond similarly is currently unknown.[27] As high doses of systemic D3 can result in hypercalcemia or anemia, our in vitro study will simulate the effect of D3 applied at the wound site and in direct contact with the HTF, similar to current application of 5-FU and MMC in glaucoma and pterygium surgeries.

Materials and Methods

Primary Culture of Human Tenon's Fibroblasts

The study was conducted according to the tenets of the Declaration of Helsinki, and approved by the Institutional Review Board of the University of Hong Kong/Hospital Authority Hong Kong West Cluster (IRB Reference Number: UW 19-366). All subjects were consecutive patients of Grantham Hospital, Hong Kong, scheduled for elective surgeries involving conjunctival dissection. We specifically recruited three types of subjects: (1) primary glaucoma patients undergoing trabeculectomy, with use of glaucoma eye drops longer than one year; (2) primary pterygium excision; (3) presumed normal without previous ocular surgery or long-term use of any eye drops (for example, eyes undergoing retinal detachment or squint surgeries).

Details of the subjects and operated eyes, where Tenon's capsules were obtained, are shown in Table 1. None of the chosen operated eyes had previous surgery involving conjunctiva or Tenon's capsule.

Tenon's capsule sample, of approximately 1 to 2 mm by 1 to 2 mm in size, was obtained during surgery and transferred immediately into tubes containing Eagle's minimum essential medium (EMEM) growth medium (ATCC, Manassas, VA, USA), supplemented with 10% bovine calf serum, 7.5 mM L-glutamine, 5 ng/mL rh-FGF-basic, 5 µg/mL rh-insulin, 1 µg/mL hydrocortisone, 50 µg/mL ascorbic acid, 100 U/mL penicillin and 100 µg/mL streptomycin. After cutting into micro pieces under sterile conditions, the samples were air-dried and seeded in a CELLSTAR 6 well cell culture plate (Greiner Bio-One, Monroe, NC, USA). The HTF were maintained in the logarithmic growth phase in 5% CO_2 humidified atmosphere at 37°C. A week after seeding, primary cultures were passaged at 60% confluence with 0.25% trypsin- ethylenediaminetetraacetic acid (EDTA; Invitrogen, Carlsbad, CA, USA) into

Table 1. Information of Sources for Tenon Tissues Used in This Study

Subject	Gender	Age	Type of Tenon	Surgery (Indication)	Ocular History
1	Male	40	Glaucoma (primary open angle glaucoma)	Trabeculectomy	Glaucoma eye drops for 1.5 years
2	Female	79	Glaucoma (primary angle closure glaucoma)	Trabeculectomy	Glaucoma eye drops for 2 years; clear cornea phacoemulsification 1 year ago
3	Male	43	Glaucoma (primary open angle glaucoma)	Trabeculectomy	Glaucoma eye drops used for 4 years
4	Male	58	Normal	Medial rectus recession (chronic abducens nerve palsy)	No previous procedures or long-term eye drop use
5	Male	61	Normal	Scleral buckling (retinal detachment)	No previous procedures or long-term eye drop use
6	Female	62	Normal	Scleral buckling (retinal detachment)	No previous procedures or long-term eye drop use
7	Male	64	Pterygium	Pterygium excision with conjunctival autograft	No previous procedures or long-term eye drop use
8	Female	65	Pterygium	Pterygium excision with conjunctival autograft	No long-term eye drop use; clear cornea phacoemulsification 6 years ago
9	Male	49	Pterygium	Pterygium excision with conjunctival autograft	No previous procedures or long-term eye drop use

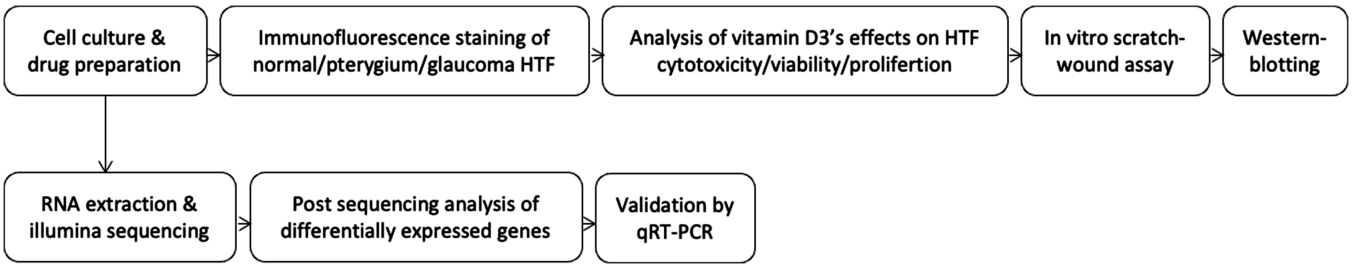

Figure 1. Experiment flow chart.

Nunc EasYFlask Cell Culture Flasks 7 5cm^2 with filter (Thermo Fisher Scientific, Waltham, MA, USA). For subsequent passaging, cells were dissociated using 0.25% trypsin-EDTA at 85%. The cultured HTF are then used in subsequent steps of the experiments as shown in Figure 1.

Immunofluorescence Staining for Identification of HTF

For immunofluorescence, HTF were seeded at a concentration of 1 × 10^5 cells/mL on 4-well Nunc Chamber Slide System (Thermo Fisher Scientific) and incubated for one day to reach a subconfluent status. Cells were fixed in cold 4% paraformaldehyde (EM GRADE; Electron Microscopy Sciences, Hatfield, PA, USA) for 10 minutes, permeabilized in 0.05% Triton X-100 (Sigma-Aldrich Corp., St. Louis, MO, USA) in phosphate-buffered saline solution (PBS) for 15 minutes, blocked in 3% bovine serum albumin in PBS for one hour, and conjugated with primary antibody in 3% bovine serum albumin/PBS (Thermo Fisher Scientific) overnight (keep cells dark in a humidified chamber) at 4°C. After incubation with secondary antibody (1:500; Thermo Fisher Scientific) for one hour at room temperature, the upper chambers were removed. Before covering with 10 mm diameter round

Table 2. Monoclonal and Polyclonal Antibodies Used in This Study

Antibody	Company	Cat
Anti-vimentin	Abcam	ab92547
Anti-alpha smooth muscle Actin	Abcam	ab5694
Anti-fibroblast Surface protein	Abcam	ab11333
Anti-Collagen I	Abcam	ab6308
Goat anti-Rabbit IgG (H+L) Cross-Adsorbed Secondary, Alexa Fluor 488	Thermo Fisher	A32731
Goat anti-Mouse IgG1 Cross-adsorbed Secondary antibody, Fluor 594	Thermo Fisher	A32742

coverslip, one drop of ibidi Mounting Medium with DAPI (4′, 6-diamidino-2-phenylindole) (ibidi USA, Fitchburg, WI, USA) was added on slides for mounting and cell nuclei staining and observed with a fluorescence microscope (Nikon ECLIPSE 80i; Nikon Inc., Melville, NY, USA) using SPOT Advanced software after 20 minutes. The antibodies used for identifying HTF in this assay are listed in Table 2.

Drug Preparations

The 1α, 25-dihydroxyvitamin D3 powder 0.1 mg (Sigma-Aldrich Corp) was dissolved in 100 µL 96% ethanol (Sigma-Aldrich Corp) and 140 µL PBS to make 1mM D3 stock and stored in −80 °C. The same volume of 96% ethanol and PBS without 1α, 25-dihydroxyvitamin D3 powder was used as a vehicle control. Mitomycin-C (MMC) powder 10 mg (Calbiochem, San Diego, CA, USA) was dissolved in 1× PBS (Thermo Fisher Scientific) to make 2.5mM MMC stock and stored in −80 °C. The drugs were diluted with culture medium to achieve the desired concentrations for the experiments.

Lactate Dehydrogenase Cytotoxic Analysis

Leakage of cytoplasmic lactate dehydrogenase (LDH) to the extracellular medium was measured with the Pierce LDH Cytotoxicity Assay Kit (Thermo Fisher Scientific), with the presence of LDH in the medium representing damage to cell membrane. LDH activity is proportional to color intensity and is expressed as optical density. For the LDH assay, 10^4 HTF/mL were seeded in each well of 96-well black wall clear bottom plates (SPL Inc., Houston, TX, USA). Twenty-four hours after cell seeding, cells in triplicate wells were exposed to different concentrations of D3 (0.001 µM, 0.01 µM, 0.1 µM, 1 µM, 5 µM, 10 µM, 25 µM, 50 µM, and 100 µM), and MMC (0.025, 0.05, 0.075, 0.1, and 0.2 mg/mL) as positive control. In addition, there were wells with corresponding concentration levels of ethanol serving as vehicle control, and cell culture medium only to correct for background color (Supplementary Methods). Absorbance was measured at a wavelength of 490 nm and 680 nm using a multimodal microplate reader (SpectraMax iD5; Molecular Devices, San Jose, CA, USA). LDH activity was determined by subtracting the 680 nm (background signal from instrument) from the 490 nm absorbance value and presented as fold-change.

PrestoBlue Cell Viability Assay

PrestoBlue Cell Viability Reagent (Invitrogen) was used for testing cell viability, based on the ability of viable cells, with active mitochondrial reductases of the electron transport chain, to convert resazurin dye (blue and nonfluorescent) to resorufin (red and highly fluorescent) (Supplementary Methods). The fluorescence is proportional to the number of viable cells and is quantified using absorbance measurements with a multimodal microplate reader (SpectraMax iD5, Molecular Devices) at 570 nm and normalized to 600 nm values.

CyQUANT Cell Proliferation Assay

Cell proliferation assays were performed using the CyQUANT Cell Proliferation Assay kit (Invitrogen) (Supplementary Methods). The samples fluorescence was measured using a multimodal microplate reader (SpectraMax iD5, Molecular Devices) at 480 nm excitation and 520 nm emission.

In Vitro Scratch Assay

Scratch assay was conducted to mimic surgical trauma and assess the subsequent migratory activity of pterygium and glaucoma HTF as part of the healing response. The HTF were grown on CELLSTAR six-well cell culture plate (Greiner

Bio-One) at the bottom outer layer of which were previously marked a cross (with 25-gauge needle) for easy recognition. When the cells reached a confluence more than 90%, the culture medium was replaced by plain EMEM medium (without serum) overnight to synchronize the cell growth. Next, the cells were stimulated with fresh EMEM medium for the blank control group, 10 µM D3/EMEM for the treatment group, the same concentrated ethanol/EMEM for the vehicle control group, 0.2 mg/mL MMC/EMEM for the positive control group for one hour. Then, the cell monolayer was scraped with a sterilized 1000 µL pipette tip to generate a cell-free gap (scratch width) in each well. After washing with PBS three times, the cells were treated again with newly made culture medium for different groups. The gap of each well was imaged randomly under inverted phase-contrast microscope (Nikon ECLIPSE TE2000-S) using SPOT Advanced software. The migration distance was evaluated quantitatively in both pterygium and glaucoma HTF treated with 10 µM D3 and the vehicle control, at 0 and 24 hours, by calculating relative scratch width (normalized to the distance at 0 hour in each group).

Western Blot Assay

After exposure to 10 µM D3/EMEM (treatment group) and the same concentration of ethanol/EMEM (vehicle control group), the cells were incubated in ice-cold RIPA Lysis Buffer (50 mM Tris-HCl, pH 7.4, 150 mM NaCl, 1% Triton X-100, 0.1% sodium dodecyl sulphate, 1% sodium deoxycholate; 10% EDTA solution, 10% protease and phosphatase inhibitor cocktail; Abcam, Cambridge, MA, USA) for 30 minutes, then centrifuged at 13,200 rpm to obtain the supernatants, which were frozen at −80°C. Protein concentrations were determined with the Pierce BCA protein assay kit (Thermo Fisher Scientific). Protein samples were separated on sodium dodecyl sulfate–polyacrylamide gel electrophoresis gels and transferred to polyvinylidene fluoride membranes, which were then probed overnight at 4°C with primary antibodies against human α smooth muscle actin (α-SMA; ab5694, 1 µg/mL; Abcam), vimentin (EPR3776; ab92547, 1:5,000; Abcam), and GADPH (sc-47724, 1:200; Santa Cruz Biotechnology, Dallas, TX, USA), followed by incubating with horseradish peroxidase–conjugated secondary antibodies (A16078, 1:20,000, Invitrogen; A6154, 1:20,000, Sigma-Aldrich Corp.) for two hours at room temperature. Labeled proteins were detected by enhanced chemiluminescence (no. 34579, Thermo Fisher Scientific).

RNA Extraction and RNA Sequencing (RNA-Seq)

Total RNA in 10 µM D3 treated HTF, as well as its vehicle and positive control, was extracted with TRIzol Reagent (Invitrogen). The integrity and purity of RNA was assessed by analyzing 260/280 nm ratios ($Ratio_{260/280}$) and 260/230 nm ratios ($Ratio_{260/230}$) on a NanoDrop One/OneC and the RNA Integrity Number (RIN) using Agilent 4200 TapeStation (Agilent Technology, Tokyo, Japan). Life Invitrogen Qubit 3.0 Fluorometer was used for quantitation of RNA sample. To construct Illumina sequencing libraries, magnetic beads with oligo-dT were used to capture the mRNA with poly A structure. Subsequently, the first strand of cDNA was synthesized in the reverse transcriptase M-MuLV (from Moloney murine leukemia virus) system with fragmented mRNA as template and random oligonucleotides as primers. Next, RNA chains were degraded by ribonuclease H (RNase H), and the second strand of cDNA was synthesized from deoxyribonucleotide triphosphates (dNTPs) in the DNA polymerase I system. After purification of double-stranded cDNA and terminal repair, A tails were added and connected to sequencing joints. About 200bp of cDNA was purified by AMPure XP beads before polymerase chain reaction (PCR) amplification. Finally, the sequencing libraries were obtained by purifying the PCR products again using AMPure XP beads. After passing the library inspection (KAPA qPCR quantification and Agilent 4200 TapeStation detection), different libraries were pooled according to the requirements of effective concentration and target disembarkation data volume, then Illumina PE150 sequencing was performed.

Post-Sequencing RNA-Seq Data Analysis

After obtaining raw data, the specific implementation process of biological information analysis was conducted (Supplementary Methods). Genes with adjusted $P < 0.05$ were considered significantly enriched by the differentially expressed genes.

Validation Via Quantitative Real-Time PCR

Total RNA was harvested using RNA spin columns (9767; Takara Biotechnology Co., Kyoto, Japan). CDNA was synthesized by reverse transcriptase from total RNA with PrimeScript RT Master Mix (RR047A; Takara Biotechnology Co.). The expression of specific mRNAs was determined with StepOnePlus Real-Time PCR System (Applied Biosystems, Foster City, CA, USA) using the TB Green Premix Ex Taq

(Tli RnaseH Plus) (RR420A; Takara Biotechnology Co., Kyoto, Japan) (Supplementary Methods).

Statistics and Mathematical Analyses

Data analysis was performed using statistical software (GraphPad Prism Version 8.0.0; GraphPad, San Diego, CA, USA). All experiments were repeated at least three times. Values were expressed as mean ± standard error (SEM). For reporting purposes, all experimental replicates using multiple subjects' samples were denoted using N = x, and the number of experimental repeats performed using each subject's sample will be denoted using n = y. The above data with more than two groups were analyzed with one-way analysis of variance. For all analyses, $P \leq 0.05$ was considered statistically significant.

Results

HTF Characterization

After HTFs migrated from the initial tissue and passaged in vitro, the cells were grown in monolayer and exhibited a spindly, generally flat, elongated shape. As shown in Figure 2, the cultured cells from all Tenon samples were positive for the antibodies chosen to confirm their HTF identity; the anti-vimentin and anti-alpha smooth muscle actin antibodies staining showed green fluorescence in the cytoplasm, the anti-collagen I and the anti-fibroblast surface protein antibodies staining showed red fluorescence, and the DAPI showed oval-shaped, blue-stained nuclei. Interestingly, the expression of myofibroblast associate markers (α-SMA and FSP) were significantly higher in pterygium and glaucoma HTF compared with presumably normal HTF from eyes undergoing vitreoretinal or squint surgeries, indicating the differentiated state of the primary cultured HTF from eyes with primary pterygium or had used topical glaucoma medication for more than one year.

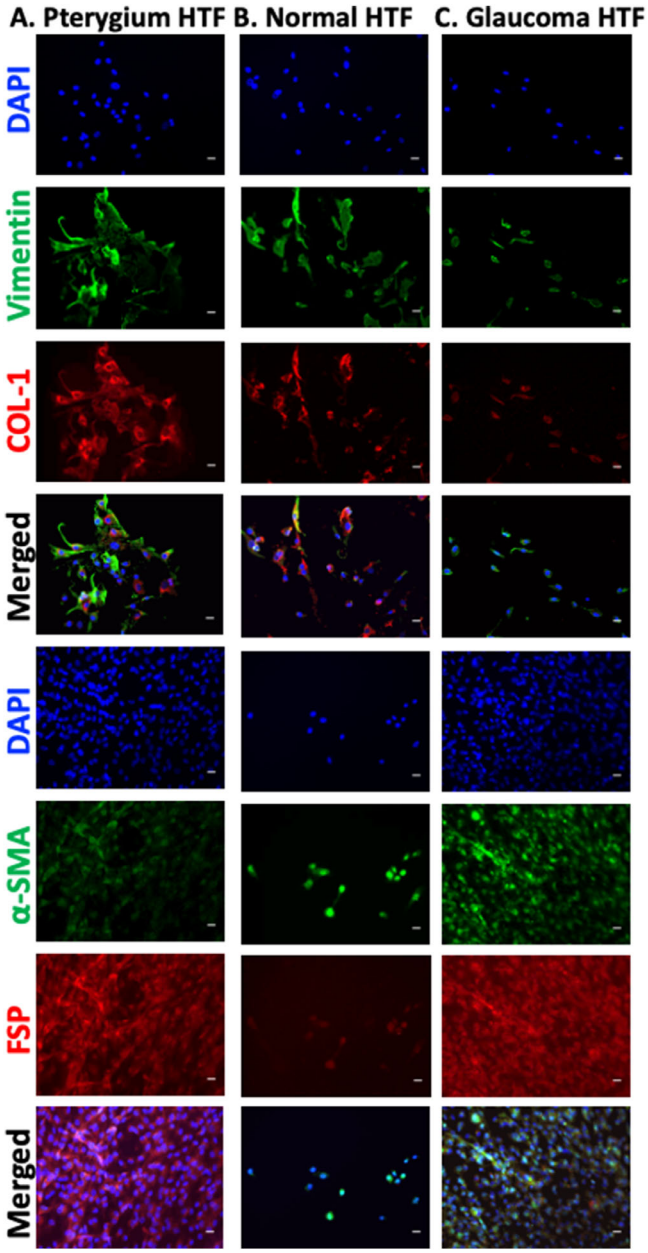

Figure 2. Primary culture cell verification. HTFs stained with Vimentin, collagen, fibroblast surface protein, α-smooth muscle actin and DAPI. (**A**) Pterygium HTF. (**B**) Normal HTF. (**C**) Glaucoma HTF (N = 3, n = 3). *Scale bar*: 25 µm

Effect of Vitamin D3 on HTF Toxicity and Cell Viability

The amount of LDH in the culture media (Figs. 3A, 3B) was stable with D3 concentrations up to the maximum tested level of 100 µM, in contrast to the incremental changes (indicating increasing cytotoxicity) noted with increasing MMC concentrations beyond the lowest level (0.025 mg/mL) tested. Similar results were seen with PrestoBlue cell viability assay, where the absorbance values at 570 nm were stable until D3 concentration was increased to 100 µM, compared to the decremental changes (indicating decreasing cellular viability) with increasing MMC concentration beyond the lowest level (0.025 mg/mL) tested. With further testing of cellular toxicity and viability using D3 at 25 µM and 50 µM on both pterygium (Figs. 3C, 3E), and glaucoma HTF (Figs. 3D, 3F), we noted LDH release increases and HTF viability decreases with concentration above 25 µM. Note that 0.025 mg/mL MMC is about one-sixteenth to

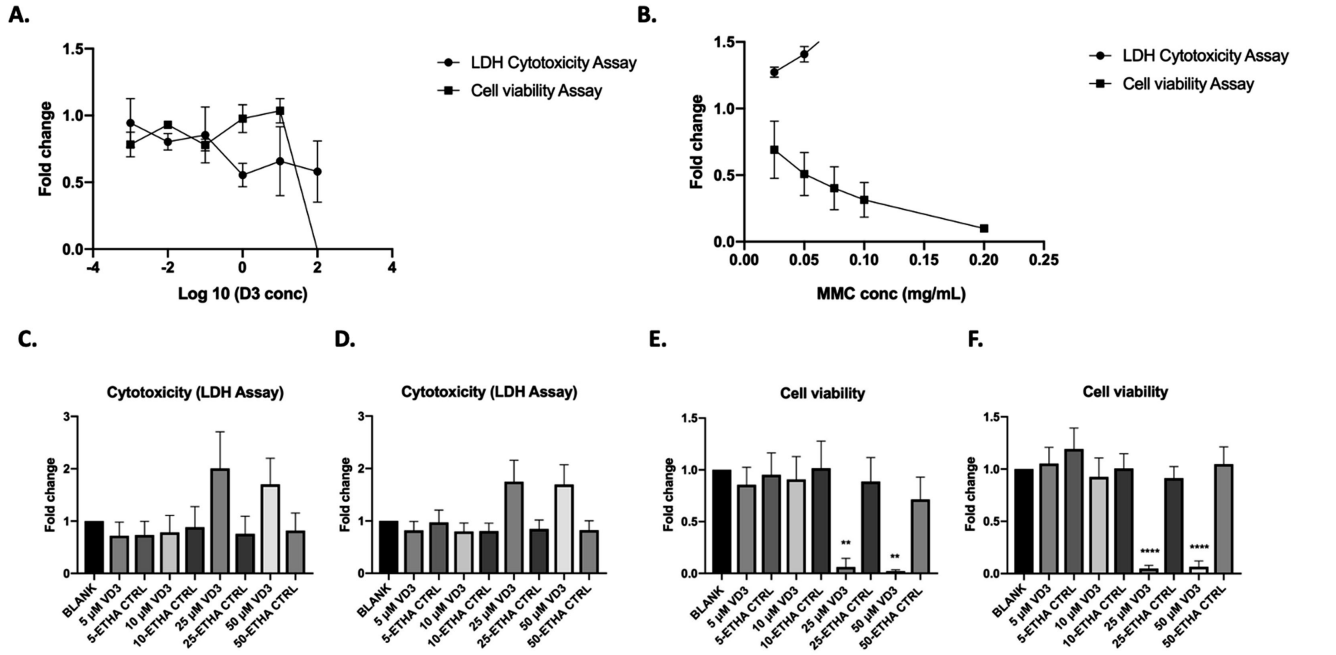

Figure 3. Cytotoxicity and cell viability evaluation on pterygium HTF using the LDH and PrestoBlue assays, respectively, to compare (**A**) the Log 10 value of different concentrations of D3 (0.001 μM to 100 μM) with (**B**) mitomycin-C (75 μM to 598 μM) (N = 1, n = 3); effect of D3 (5 μM to 50 μM) on (**C**) pterygium HTF cytotoxicity and (**D**) glaucoma HTF cytotoxicity (N = 3 , n = 3); and effect of D3 (5 μM to 50 μM) on (**E**) pterygium HTF viability and (**F**) glaucoma HTF viability (N = 3 , n = 3). The *arrows* indicate clinically used MMC concentration of 0.1 and 0.2 mg/mL, equivalent to 299 and 598 μM. (**$P \leq 0.05$; ****$P \leq 0.001$)

one-eighth of the concentration used clinically in pterygium and glaucoma surgeries.

Vitamin D3 Inhibits HTF Proliferation, Migration, and Transdifferentiation to Myofibroblasts

Cell proliferation assessment by the CyQuant assay showed D3 treatment significantly decreased HTF proliferation after 24 hours, in a dose-dependent manner (Figs. 4A, 4B).

In the scratch wound assays, cell migration was relatively fast in the control groups, with significant reduction of scratch width at 24 hours, in contrast to the D3 (10 μM) and MMC (0.2 mg/mL) treated groups, where it was not significantly different from 0 hour (immediately after scratching), as shown in Figures 4C and 4D, indicating suppression of cell migration. We also noted that the HTF started to float within the first hour in the MMC group, which was suggestive of cell death, although this was not observed in the blank, D3, or vehicle control groups. As shown in Figures 4E and 4F, simulated wound closure by HTF was significantly suppressed by 10 μM D3 treatment compared with the vehicle control.

Because the accumulation of ECM proteins is an indicator of myofibroblast transdifferentiation, we evaluated the effect of D3 on expression of α-SMA, an ECM component, using Western blots. As shown in Figure 4G, D3 treatment strongly inhibited α-SMA expression in both pterygium and glaucoma HTF.

The Molecular Pathology of HTF

To further investigate the molecular pathology of pterygium and glaucoma HTF, we compared the transcriptional profiles of pterygium (n = 4) and glaucoma (n = 4) versus normal (n = 1) conjunctival tissues by RNA-seq. Based on the RNA-seq data, both glaucoma and pterygium cases showed completely different expression patterns compared to that of the normal tissue (Figs. 5A, 5B). To explore the pathological process of glaucoma and pterygium HTF, we combined two differentially expressed genes (DEGs) by Venn diagram (Fig. 5C). Among these DEGs, 8642 transcripts both changed in the disease group against the normal. The top 20 genes with the most obvious expression changes based on adjusted *P* values are listed in Table 3 and Table 4.

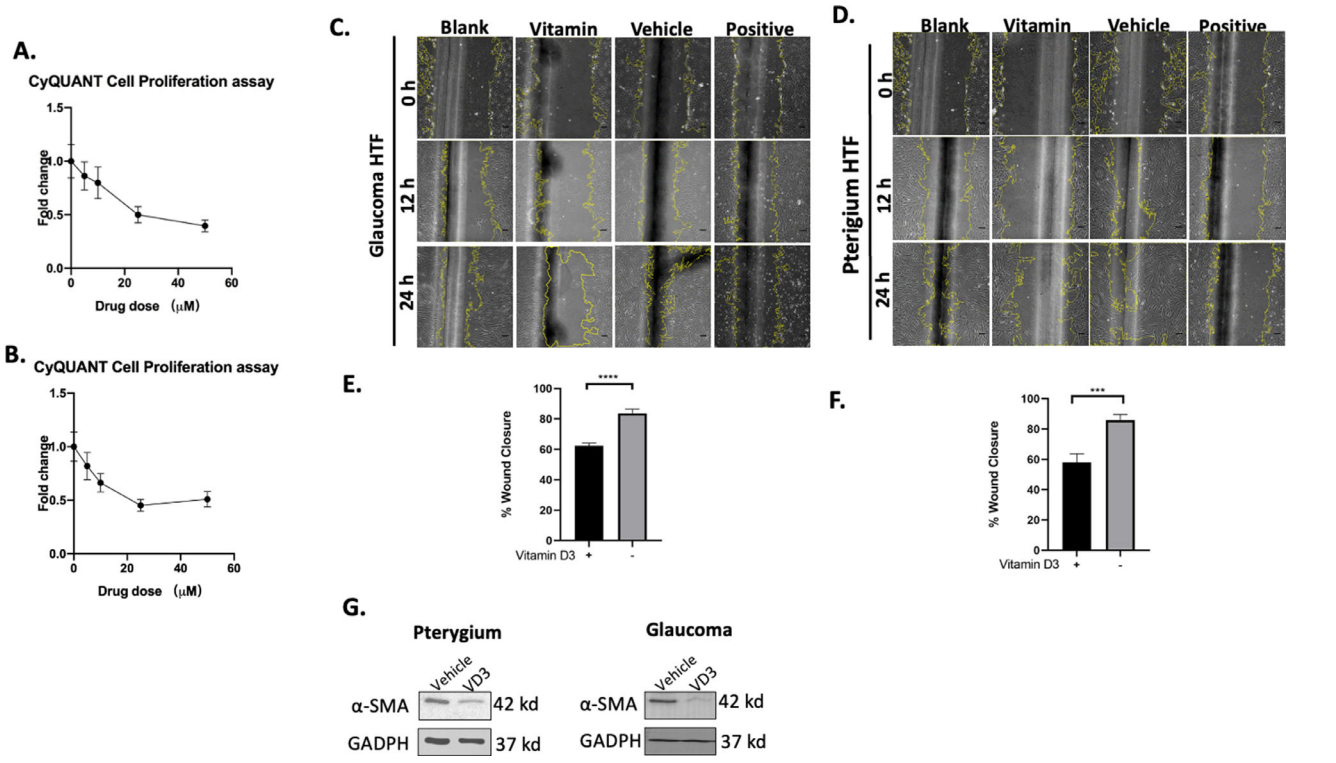

Figure 4. Inhibition of proliferation in (**A**) pterygium HTF and (**B**) glaucoma HTF seeded at 10,000 cells/well in a 96-well plate and grown for 24 hours in presence of ethanol or increasing concentrations of D3. Relative proliferation was measured by fluorescence determination of DNA content using the CyQuant Proliferation assay (N = 3, n = 3). Representative images of D3-induced inhibition of wound healing in (**C**) pterygium HTF and (**D**) glaucoma HTF as compared to the EMEM, ethanol (vehicle control), and MMC (positive control, 598 μM) at 0, 12, and 24 hours after scratch (*Scale bar*: 100 μm). Cell migration was evaluated quantitatively in (**E**) pterygium cases (N = 3, n = 4) and (**F**) glaucoma cases (N = 3, n = 3) respectively, between 10 μM D3-treated HTF and the vehicle control HTF at 0 and 24 hours by calculating relative wound closure percentage. Data are presented as the means ± SEM (***$P < 0.001$; ****$P < 0.0001$, compared with vehicle control group). (**G**) The expression of α-smooth muscle actin (α-SMA) was evaluated using Western blots.

Vitamin D3 Enhances CYP24A1, SHE, KRT16 But Suppresses CILP Expression in HTF

To further investigate the mechanism of effect by D3 on HTF, we performed RNA-seq analysis for pterygium, glaucoma, and normal HTF. This consists of normal blank control (*normal_bl*; n = 1), pterygium blank control (*ptery_bl_1*; n = 1), glaucoma blank control (*glau_bl_1*; n = 1), pterygium MMC positive control (*ptery_MMC_1*; n =1), glaucoma MMC positive control (*glau_MMC_1*; n = 1), pterygium vehicle control (*ptery_veh_1, ptery_veh_2, ptery_veh_3*; n = 3), glaucoma vehicle control (*glau_veh_1, glau_veh_2, glau_veh_3*; n = 3), pterygium treated with D3 (*ptery_vD3_1, ptery_vD3_2, ptery_vD3_3*; n = 3), and glaucoma treated with D3 (*glau_vD3_1, glau_vD3_2, glau_vD3_3*; n = 3). To eliminate any outliers, both principal-component analysis and hierarchical clustering were applied to segregate the transcriptomic profiles of vehicle (veh) from D3-treated (D3) pterygium and glaucoma HTF, leaving seven samples demonstrating the greatest difference between the vehicle and D3 group (i.e., *glau_veh_1, glau_veh_2, ptery_veh_2, ptery_veh_3, glau_vD3_2, ptery_vD3_2, ptery_vD3_3*) (Figs. 6A, 6B). Differential expression analysis of these samples revealed 4251 DEGs in the D3-treated group compared with the vehicle group. The top 10 genes were displayed in volcano plot (Fig. 6C). Two of the upregulated genes, *CYP24A1* and *KRT16*, were selected for PCR verification, which appeared consistent with the RNA-seq data (Figs. 6D, 6E).

To gain further insight into the various targets and their associated pathways, we performed pathway enrichment analysis of the differently expressed sequences' target genes based on the GO/KEGG database. By subjecting the differentially expressed genes from the group of D3 and vehicle control in both glaucoma and pterygium HTF, we observed numerous enriched gene sets. During the GO enrichment analysis, the genes were mainly enriched in extracellular matrix organization, extracellular

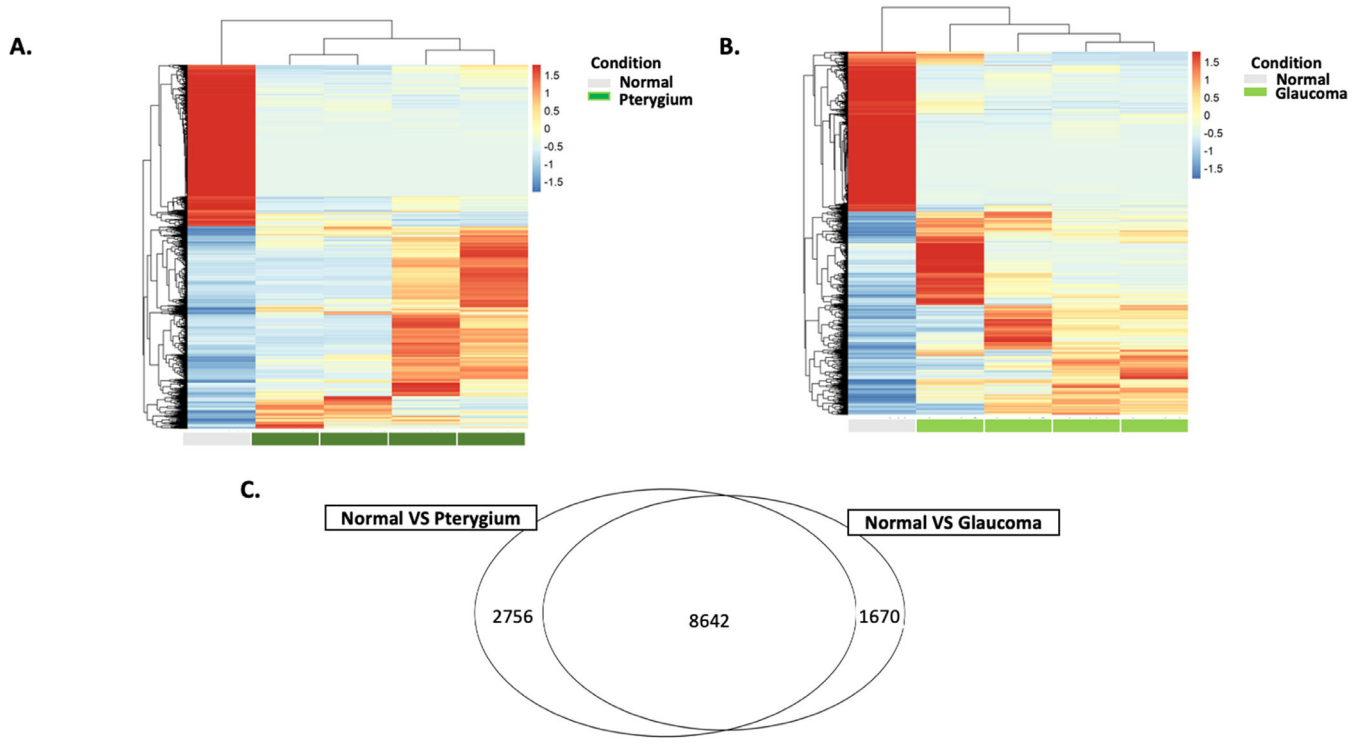

Figure 5. (**A**) Hierarchical clustering of all DEGs between the normal and the pterygium. (**B**) Hierarchical clustering of all DEGs between the normal and the glaucoma. Expression values are Z score transformed. Samples were clustered using complete linkage and Euclidean distance. (**C**) Venn diagram of DEGs that both changed ($P < 0.05$) in the pterygium and glaucoma in comparison to that of the normal.

structure organization and homophilic cell adhesion via plasma membrane adhesion molecules (Fig. 6F). We further investigated the functional implications of these differentially expressed genes of D3 treatment by KEGG pathway analysis. A number of the differentially expressed genes were enriched in four KEGG pathways, including calcium signaling pathway, retrograde endocannabinoid signaling, inflammatory mediator regulation of TRP channels and AGE-RAGE signaling pathway in diabetic complications ($P < 0.05$) (Fig. 6G). Because MMC is commonly used as an antifibrotic agent during pterygium and glaucoma surgery, we compared the effect of D3 and MMC on HTF by analyzing their DEGs by Venn diagram. As shown in Figure 7A, a total of 533 DEGs were obtained from comparison between D3/MMC and the vehicle group, and these genes reached the threshold P value <0.05. Among these DEGs, *CYP24A1* showed changes in both D3 and MMC treated group. In the pterygium group, it showed that *KCNE4*, *GDPD5*, *TDRD10*, *SHE*, *HSPG2*, *CILP*, *CLMN*, *SULT1C2*, *MLXIPL* changed in both D3 and MMC group, while *IL11*, *GDF15*, *ATF3*, *STC1*, *ADAMTS15*, *HBEGF*, *PMAIP1* were found to change in the glaucoma group. Among these genes, we selected *SHE* and *CILP* to conduct PCR verification using pterygium HTF (Fig. 7B). The real-time PCR results showed that D3 could significantly upregulate *SHE* and downregulate *CILP* in pterygium HTF.

Discussion

The outcome of ocular procedures like glaucoma filtration surgery (trabeculectomy) and pterygium excision are closely dependent on the postoperative response of subconjunctival Tenon's fibroblasts.[28] Therefore the inhibition of excessive proliferation and migration of HTF continues to be a key goal for improving surgical success.[29] However, the use of current antifibrotic agents such as MMC and 5-FU involves off-label use of cytotoxic agents with potentially serious complications including bleb leak, blebitis, and endophthalmitis after trabeculectomy, and corneoscleral melt after pterygium excision.[30,31]

Our study showed that D3 had a regulatory effect on the activity of subconjunctival fibroblasts, similar to their previously reported effect on cutaneous fibroblasts. At concentration up to 25 µM, D3 also appears safer than MMC, currently the most commonly used antifibrotic agent, even at concentration well below clinical usage. However, D3 appears to be cytotoxic at

Table 3. Top 20 DEGs of HTFs Versus Normal

Gene Name	Ensembl ID	logFC	logCPM	*P* Value	FDR	padj
IGFBP5	ENSG00000115461	9.304032	10.76389	1.38E-203	6.78E-199	6.78E-199
ADAM33	ENSG00000149451	16.9437	9.171072	1.40E-188	3.43E-184	3.43E-184
KRT14	ENSG00000186847	−8.45785	2.493931	1.67E-182	2.73E-178	2.73E-178
MFAP4	ENSG00000166482	16.48898	8.71592	4.88E-175	5.98E-171	5.98E-171
C1R	ENSG00000159403	16.39318	8.620644	3.36E-172	3.29E-168	3.29E-168
UNC13A	ENSG00000130477	−7.2974	2.578969	1.33E-166	9.32E-163	9.32E-163
FBLN1	ENSG00000077942	7.275678	11.16998	3.85E-165	2.36E-161	2.36E-161
C1S	ENSG00000182326	8.187354	8.609866	2.40E-152	1.31E-148	1.31E-148
SOD3	ENSG00000109610	15.57047	7.79558	7.44E-148	3.31E-144	3.31E-144
ADH1B	ENSG00000196616	6.690222	10.60805	8.34E-148	3.41E-144	3.41E-144
APOD	ENSG00000189058	15.55709	7.78453	1.68E-147	6.33E-144	6.33E-144
FBN2	ENSG00000138829	6.808775	9.189304	3.38E-140	1.18E-136	1.18E-136
COL15A1	ENSG00000204291	8.374811	7.799208	5.59E-137	1.71E-133	1.71E-133
GPNMB	ENSG00000136235	7.184093	8.020785	2.18E-130	6.28E-127	6.28E-127
ODC1	ENSG00000115758	−3.49122	6.271205	3.25E-130	8.84E-127	8.84E-127
MXRA5	ENSG00000101825	14.88263	7.106794	1.54E-128	3.98E-125	3.98E-125
APOE	ENSG00000130203	14.81225	7.043766	1.32E-126	3.25E-123	3.25E-123
PTGIS	ENSG00000124212	6.895927	7.955062	8.62E-126	2.01E-122	2.01E-122
COL3A1	ENSG00000168542	5.695702	12.07477	2.78E-125	6.19E-122	6.19E-122
FOXC2	ENSG00000176692	−4.11519	3.875123	5.47E-124	1.17E-120	1.17E-120

Table 4. Top 20 DEGs for MMC and VD3 Versus Vehicle

Gene Name	Ensembl ID	*P* Value	padj	Style
MCAM	ENSG00000076706	2.03E-06	0.000949	Down
SH2D2A	ENSG00000027869	1.78E-07	0.000144	Down
C3orf52	ENSG00000114529	1.05E-05	0.003362	Down
AC004520.1	ENSG00000273237	3.21E-06	0.001348	Down
TREM2	ENSG00000095970	0.000109	0.018255	Down
SERPINB2	ENSG00000197632	3.95E-14	1.87E-10	Down
SERPIND1	ENSG00000099937	1.05E-09	1.75E-06	Down
DUSP4	ENSG00000120875	9.61E-05	0.016812	Down
E2F7	ENSG00000165891	6.52E-12	1.94E-08	Down
ICAM1	ENSG00000090339	7.12E-07	0.00042	Down
AMIGO2	ENSG00000139211	3.31E-06	0.00138	Down
SLC52A1	ENSG00000132517	2.46E-08	2.58E-05	Down
MMP1	ENSG00000196611	2.20E-13	8.91E-10	Down
MMP3	ENSG00000149968	6.00E-11	1.48E-07	Down
AC026803.2	ENSG00000267898	2.44E-07	0.000184	Down
SENCR	ENSG00000254703	1.44E-05	0.004241	Down
AL356215.1	ENSG00000255521	1.71E-05	0.004711	Down
AADACP1	ENSG00000240602	3.08E-07	0.000221	Down
KIF26B	ENSG00000162849	0.00014	0.021553	Up
GCSAM	ENSG00000174500	3.58E-06	0.001469	Down

concentration above 25 μM. Our CyQuant proliferation assays on glaucoma and pterygium HTF treated with D3 for 24 hours showed that it could suppress HTF proliferation in a dose-dependent manner. We believe that the optimal concentration of D3 is around 10 to 25 μM, with regard to cellular safety and inhibitory effect on HTF proliferation. In our Western blot analysis of ECM components, α-SMA

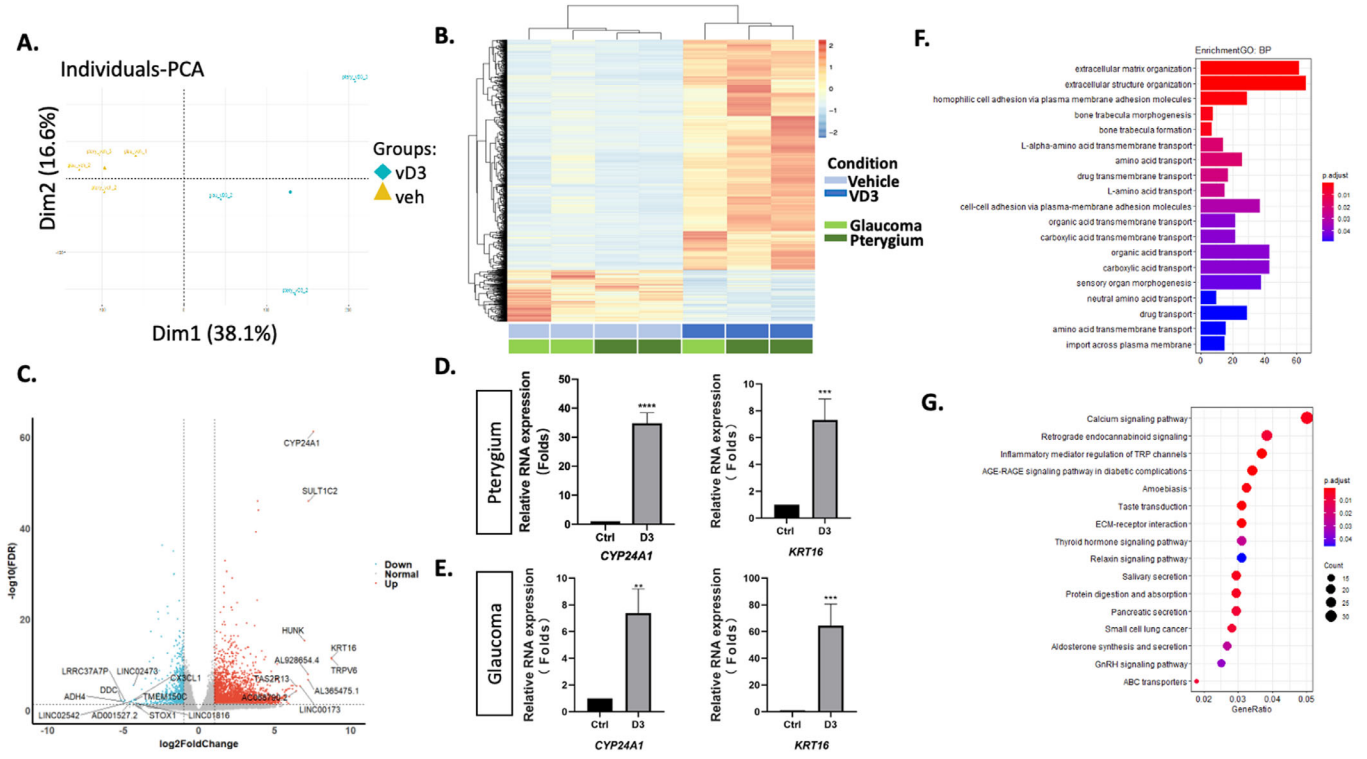

Figure 6. (**A**) Principal-component analysis (PCA) plot of n = 4251 genes expressed in the D3-treated group (n = 3) and the vehicle group (veh) (n = 4). (**B**) Hierarchical clustering of all DEGs between the D3 and the vehicle groups. Expression values are Z score transformed. Samples were clustered using complete linkage and Euclidean distance. (**C**) Volcano plots for DEGs between the D3-treated and the vehicle groups. As observed in the figure, the upregulated and downregulated genes were marked as a *dot*, those significantly up-regulated genes were highlighted in *red*, the down-regulated genes were highlighted in *blue*, and the nonsignificant genes were labeled as *gray dots*. In the figure, the *gray lines* indicate the marginal lines separating DEGs from non-DEGs, with the *horizontal lines* denoting the *P* value threshold ($P \leq 0.05$). The top 10 upregulated and downregulated genes were showed in graph: pterygium (**D**) and glaucoma (**E**) treated with 10 µM D3 or vehicle for 24 hours. Then mRNA expressions of *CYP24A1*, *KRT16* in pterygium and glaucoma were measured by qPCR and normalized to *GAPDH* (n = 3). The vehicle and D3-treated groups consist of primary cultured pterygium or glaucoma HTF that are not treated or treated with specific concentration of D3, respectively. All bar graphs are expressed as mean ± SEM (***$P < 0.001$; ****$P < 0.0001$). (**F**) GO analysis of DEGs between the D3-treated and the vehicle groups. The graph displays the classification term enrichment status and term hierarchy. The color scale shows the *P* value cutoff levels for each biological process. (**G**) KEGG analysis of DEGs between the D3-treated and the vehicle groups. The color scale shows the *P* value, and the dot size shows the related DEGs.

expression was reduced after D3 treatment, indicating suppressed myofibroblast transdifferentiation. In 2007, Albert et al. also demonstrated that calcitriol (1α,25(OH)2D3) concentrations ≥50 µM can significantly decrease endothelial cell viability in retinal capillaries.[32] A limitation of our study was that MMC and D3 concentrations may not be strictly maintained during the entire experiment (24 hours), because of their degradable properties when exposed to light or relatively high temperature.

For our mRNA profile analysis, although we imported data from 17 samples, we only performed further analysis for seven samples (i.e., *glau_veh_1, glau_veh_2, ptery_veh_2, ptery_veh_3, glau_vD3_2, ptery_vD3_2, ptery_vD3_3*), because these clustered the best to display the difference between the vehicle and D3 group. Our qPCR result was consistent with that of RNA-seq.

In 2016, Srikuea et al.[33] reported administration of 1α,25(OH)2D3 at a supra-physiological dose can decrease satellite cell differentiation, delay regenerative muscle fiber formation, and increase muscular fibrosis. The 1α,25(OH)2D3 has been reported to activate intracellular signaling molecules such as protein kinases A and C, phosphatidylinositol 3-kinase, phospholipase C, as well as open calcium channels in addition to transcriptional activation.[34] The concentration of 1α,25(OH)2D3 is regulated by the action of the vitamin D3-catabolizing enzyme, encoded by the CYP24A1 gene, to convert it to the inactive metabolite, calcitroic acid.[35] As one of the major enzymes regulating D3, the upregulation of

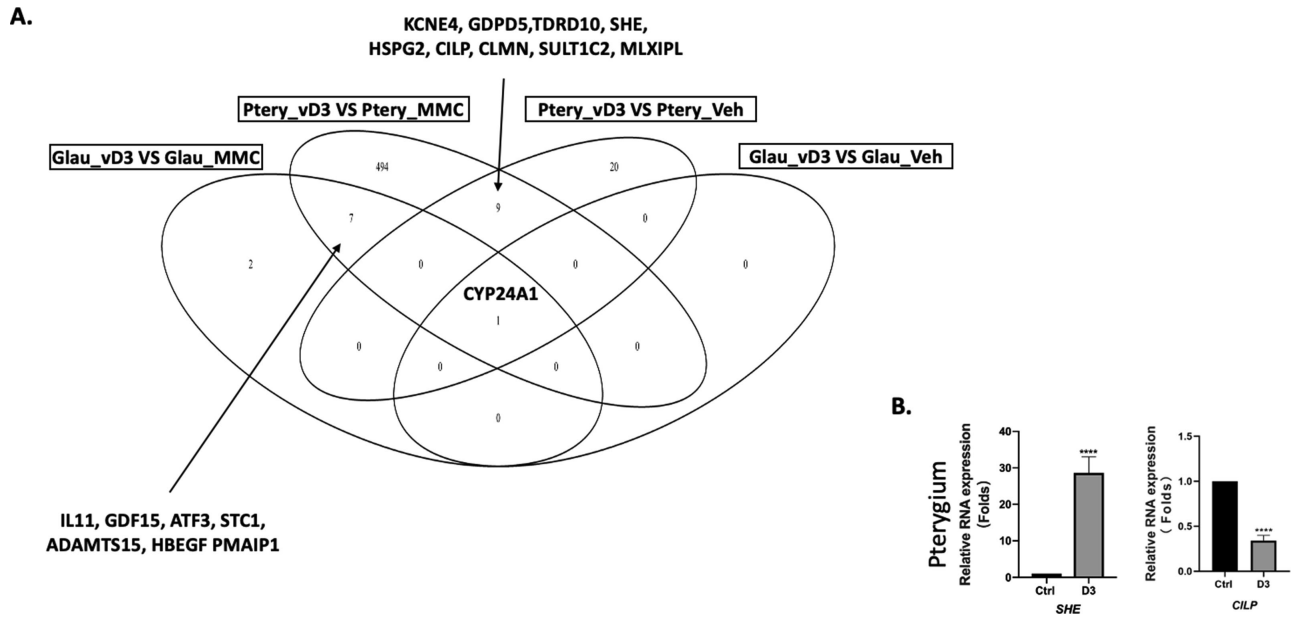

Figure 7. (**A**) Venn diagram showing DEGs that are both changed in vitamin D3 (vD3)– and MMC-treated, compared to normal, tissues. (**B**) Pterygium HTF were treated with 10 µM vD3 or vehicle for 24 hours, then mRNA expression of *SHE*, *CILP* were measured by qPCR and normalize to *GAPDH* (n = 3). All bar graphs are expressed as mean ± SEM. (*$P < 0.5$; ***$P < 0.001$; ****$P < 0.0001$).

CYP24A1 in D3 treated HTF confirms the presence of local metabolism of 1α,25(OH)2D3.

SHE (Src Homology 2 Domain Containing E) belongs to the Src homology 2 (SH2) domain family. SHE is reported to be associated with diseases such as blepharoconjunctivitis.[36] It is now known that the human genome encodes ~120 SH2 domains that are dispersed in more than 110 proteins.[37] These include protein or lipid kinases, protein phosphatases, small GTPases, cytoskeleton regulators, and adaptor/scaffolding proteins and other regulators of signal transduction.[38] For example, Src homology 2 domain-containing inositol 5′-phosphatase is a negative regulator of the phosphatidylinositol 3-kinase/protein kinase B (PI3K/Akt) signaling.[39] In 2017, Li et al. suggests that decreased Src homology 2 domain-containing inositol 5′-phosphatase mediates high glucose-induced TGF-β1 upregulation and ECM deposition through activation of the PI3K/Akt pathway in renal tubular cells.[40] PI (3,4,5) P3 initiates a variety of signaling cascades by interacting with pleckstrin homology (PH) domain-containing proteins, most notably the serine kinase Akt.[41] The activity of the PI3K/Akt signaling axis is multifunctional and is involved in renal ECM accumulation and interstitial fibrosis.[40] The upregulation of SHE after treatment with D3 may suggest suppression of TGF-β1 induced subconjunctival fibrosis via PI3K/Akt signaling axis.

Keratin 16 (K16), a type I cytokeratin encoded by the *KRT16* gene, when paired with keratin 6 in epithelial tissues, was found to maintain collective cell adhesion and integrity by increasing cell-cell and cell-matrix contact and decreasing cell migration and directionality during skin wounding.[42] In 2010, Nima Aden et al. confirmed that in systemic sclerosis, epidermal keratinocytes have a delayed differentiation and expression of K16.[43] In the same year, Trost et al. investigated on the influence of excess K16 on the migratory behavior of HaCaT keratinocytes in vitro and found that cells overexpressing K16 displayed a 90% reduction in migration potential compared to mock-transfected immortalized human keratinocytes.[44] In our study, D3 treatment significantly upregulates *KRT16* gene expression, and possibly leading to enhanced cellular adhesion and migration suppression.

Cartilage intermediate layer protein (CILP) is a key regulator of cardiac remodeling and heart failure.[45] In 2018, Zhang et al. reported that CILP-1 alleviates pressure overload-induced cardiac fibrosis via interfering with TGF-β1 signaling and concluded that CILP-1 is a novel ECM protein possessing antifibrotic ability in pressure overload-induced fibrotic remodeling.[45] They demonstrated that C-terminal CILP-1 increased Akt phosphorylation, promoted the interaction between Akt and Smad3, and suppressed Smad3 phosphorylation.[45] The antifibrotic effect of CILP-1 is attributed to it interfering with TGF-β1 signaling through its

N- and C- terminal fragments.[46] Blockade of PI3K-Akt pathway attenuated the inhibitory effect of C-CILP-1 on TGF-β1-induced Smad3 activation.[45] The downregulation of CILP may indicate lower fibrotic remodeling.

Apart from the qPCR validation results, our mRNA profiles revealed some candidate genes like IGFBP-5, ADAM33 and KRT14 (Table 3.), which have been reported to play vital roles in fibrosis or ECM reconstruction.[47–49] In addition, vitamin D3 could significantly downregulated chemokine *CXCL1*, retinol metabolic related gene *ADH4* (Fig. 6C). It appears that further investigation of the possible regulatory effect of these candidate genes is warranted. Both RNA-seq and qPCR data suggest that D3 affects not only scar tissue hyperplasia but also the inflammatory response after tissue injury. We hope to validate these effects of D3 in a future, in vivo, filtration surgery animal model, which will allow us to further study the effect of different mode of administration (subconjunctival injection or topical application), frequency of administration (intraoperative or perioperative), and its effect on adjacent tissues (for example, corneal and conjunctival epithelium).

Conclusions

This study showed for the first time that D3 appears capable of suppressing HTF proliferation, migration, and transdifferentiation, and these effects are mediated by its ability to promote the expression of the *CYP24A1, KRT16,* and *SHE* genes, while suppressing *CILP* gene expression. Clinically, D3 may have an important role in preventing subconjunctival fibrosis after surgery involving conjunctiva and Tenon's capsule and possibly improving their postoperative outcome, especially for lowering recurrences after pterygium excision and maintaining aqueous filtration after trabeculectomies.

Acknowledgments

Supported by Seed Fund for Basic Research, University Research Committee, the University of Hong Kong.

Disclosure: **S. Jia,** None; **F. Chen,** None; **H. Wang,** None; **G. Kesavamoorthy,** None; **J.S.M. Lai,** None; **I.Y.H. Wong,** None; **K. Chiu,** None; **J.C.H. Chan,** None

References

1. Tham YC, Li X, Wong TY, Quigley HA, Aung T, Cheng CY. Global prevalence of glaucoma and projections of glaucoma burden through 2040: a systematic review and meta-analysis. *Ophthalmology*. 2014;121:2081–2090.
2. Burk RO, Rohrschneidern K, Noack H, Völcker HE. Are large optic nerve heads susceptible to glaucomatous damage at normal intraocular pressure? *Graefes Arch Clin Exp Ophthalmol*. 1992;230:552–560.
3. Miller PE. The glaucomas. In: Maggs D, Miller P, Ofri R, eds. *Slatter's fundamentals of veterinary ophthalmology*. St. Louis: Elsevier; 2007:230–257.
4. Fechtner RD, Realini T. Fixed combinations of topical glaucoma medications. *Curr Opin Ophthalmol*. 2004;15:132–135.
5. Sidoti PA, Dunphy TR, Baerveldt G, et al. Experience with the Baerveldt glaucoma implant in treating neovascular glaucoma. *Ophthalmology*. 1995;102:1107–1118.
6. Bill AN. Blood circulation and fluid dynamics in the eye. *Physiol Rev*. 1975;55:383–417.
7. Tu H, Smedley GT, Haffner D, Niksch BA, Inventors; Glaukos Corp, assignee. Glaucoma stent and methods thereof for glaucoma treatment. United States patent US 7,135,009. 2006 Nov 14.
8. Cotlear D, Melamed S. Incisional therapies: trabeculectomy surgery. In: Samples JR, Schacknow PN, ed. *Clinical Glaucoma Care*. New York: Springer; 2014:541–570.
9. Zhang Z, Ma J, Yao K, Yin J. Alpha-melanocyte stimulating hormone suppresses the proliferation of human tenon's capsule fibroblast proliferation induced by transforming growth factor beta 1. *Mol. Biol*. 2012;46:563–568.
10. Liu Y, Kimura K, Orita T, et al. Inhibition by a retinoic acid receptor γ agonist of extracellular matrix remodeling mediated by human Tenon fibroblasts. *Mol Vis*. 2015;21:1368.
11. Wilson SL, El Haj AJ, Yang Y. Control of scar tissue formation in the cornea: strategies in clinical and corneal tissue engineering. *J Funct Biomater*. 2012;3:642–687.
12. Manning CA, Kloess PM, Diaz MD, Yee RW. Intraoperative mitomycin in primary pterygium excision: a prospective, randomized trial. *Ophthalmology*. 1997;104:844–848.
13. Koppaka V. *Investigating the role of aldehyde dehydrogenase 3A1 in regulation of corneal epithelial homeostasis*. Aurora, CO: University of Colorado

Anschutz Medical Campus; 2013. Doctoral dissertation.
14. Seibold LK, Sherwood MB, Kahook MY. Wound modulation after filtration surgery. *Surv Ophthalmol*. 2012;57:530–550.
15. Aswin PR. *Outcome of glaucoma surgery in patients on prostaglandin analogues*. Madurai, India: Aravind Eye Hospital and Post Graduate Institute of Ophthalmology; 2018. Doctoral dissertation.
16. Baudouin C. Detrimental effect of preservatives in eyedrops: implications for the treatment of glaucoma. *Acta Ophthalmol (Copenh)*. 2008;86:716–726.
17. Schuster I. Cytochromes P450 are essential players in the vitamin D signaling system. *Biochim Biophys Acta*. 2011;1814:186–199.
18. Reins RY, McDermott AM. Vitamin D: implications for ocular disease and therapeutic potential. *Exp Eye Res.* 2015;134:101–110.
19. de Haan JB, Bladier C, Griffiths P, et al. Mice with a homozygous null mutation for the most abundant glutathione peroxidase, Gpx1, show increased susceptibility to the oxidative stress-inducing agents paraquat and hydrogen peroxide. *J Biol Chem*. 1998;273:22528–22536.
20. Shokravi MT, Marcus DM, Alroy J, Egan K, Saornil MA, Albert DM. Vitamin D inhibits angiogenesis in transgenic murine retinoblastoma. *Invest Ophthalmol Vis Sci*. 1995;36:83–87.
21. Suzuki T, Sano Y, Kinoshita S. Effects of 1α, 25-dihydroxyvitamin D3 on Langerhans cell migration and corneal neovascularization in mice. *Invest Ophthalmol Vis Sci*. 2000;41:154–158.
22. Albert DM, Scheef EA, Wang S, et al. Calcitriol is a potent inhibitor of retinal neovascularization. *Invest Ophthalmol Vis Sci*. 2007;48:2327–2334.
23. Tang J, Zhou RU, Luger D, et al. Calcitriol suppresses antiretinal autoimmunity through inhibitory effects on the Th17 effector response. *J Immunol.* 2009;182:4624–4632.
24. Lee V, Rekhi E, Kam JH, Jeffery G. Vitamin D rejuvenates aging eyes by reducing inflammation, clearing amyloid beta and improving visual function. *Neurobiol Aging*. 2012;33:2382–2389.
25. Kutuzova GD, B'Ann TG, Kiland JA, Hennes-Beann EA, Kaufman PL, DeLuca HF. 1α, 25-Dihydroxyvitamin D3 and its analog, 2-methylene-19-nor-(20S)-1α, 25-dihydroxyvitamin D3 (2MD), suppress intraocular pressure in non-human primates. *Arch Biochem Biophys.* 2012;518:53–60.
26. Sriram G, Bigliardi PL, Bigliardi-Qi M. Fibroblast heterogeneity and its implications for engineering organotypic skin models in vitro. *Eur J Cell Biol.* 2015;94:483–512.
27. Siak JJ, Ng SL, Seet LF, Beuerman RW, Tong L. The nuclear-factor κB pathway is activated in pterygium. *Invest Ophthalmol Vis Sci.* 2011;52:230–236.
28. Lama PJ, Fechtner RD. Antifibrotics and wound healing in glaucoma surgery. *Surv Ophthalmol.* 2003;48:314–346.
29. Stahnke T, Kowtharapu BS, Stachs O, et al. Suppression of TGF-β pathway by pirfenidone decreases extracellular matrix deposition in ocular fibroblasts in vitro. *PLoS One*. 2017;12(2):e0172592.
30. Bindlish R, Condon GP, Schlosser JD, D'Antonio J, Lauer KB, Lehrer R. Efficacy and safety of mitomycin-C in primary trabeculectomy: five-year follow-up. *Ophthalmology*. 2002;109:1336–1341.
31. Tsai YY, Lin JM, Shy JD. Acute scleral thinning after pterygium excision with intraoperative mitomycin C: a case report of scleral dellen after bare sclera technique and review of the literature. *Cornea*. 2002;21:227–229.
32. Albert DM, Scheef EA, Wang S, et al. Calcitriol is a potent inhibitor of retinal neovascularization. *Invest Ophthalmol Vis Sci.* 2007;48:2327–2334.
33. Srikuea R, Hirunsai M. Effects of intramuscular administration of 1α, 25 (OH) 2D3 during skeletal muscle regeneration on regenerative capacity, muscular fibrosis, and angiogenesis. *J Appl Physiol.* 2016;120:1381–1393.
34. Deeb KK, Trump DL, Johnson CS. Vitamin D signalling pathways in cancer: potential for anticancer therapeutics. *Nat Rev Cancer*. 2007;7:684–700.
35. Schlingmann KP, Kaufmann M, Weber S, et al. Mutations in CYP24A1 and idiopathic infantile hypercalcemia. *N Engl J Med.* 2011;365:410–421.
36. Kaneko T, Joshi R, Feller SM, Li SS. Phosphotyrosine recognition domains: the typical, the atypical and the versatile. *Cell Commun Signal*. 2012;10:32.
37. Doolittle RF. The multiplicity of domains in proteins. *Annu Rev Biochem*. 1995;64:287–314.
38. Zheng Y. Dbl family guanine nucleotide exchange factors. *Trends Biochem. Sci*. 2001;26:724–732.
39. Martini M, De Santis MC, Braccini L, Gulluni F, Hirsch E. PI3K/AKT signaling pathway and cancer: an updated review. *Ann Med.* 2014;46:372–383.
40. Li F, Li L, Hao J, Liu S, Duan H. Src homology 2 domain-containing inositol 5′-phosphatase ameliorates high glucose-induced extracellular matrix deposition via the phosphatidylinositol 3-kinase/protein kinase b pathway in renal tubular epithelial cells. *J Cell Biochem*. 2017;118:2271–2284.

41. Dowler S, Currie RA, Campbell DG, et al. Identification of pleckstrin-homology-domain-containing proteins with novel phosphoinositide-binding specificities. *Biochem J.* 2000;351:19–31.
42. Zhang X, Yin M, Zhang LJ. Keratin 6, 16 and 17—critical barrier alarmin molecules in skin wounds and psoriasis. *Cells*. 2019;8:807.
43. Aden N, Nuttall A, Shiwen X, et al. Epithelial cells promote fibroblast activation via IL-1α in systemic sclerosis. *J Invest Dermatol.* 2010;130:2191–2200.
44. Trost A, Costa I, Jakab M, et al. K16 is a further new candidate for homotypic intermediate filament protein interactions. *Exp Dermatol*. 2010;19(8):e241–e250.
45. Zhang CL, Zhao Q, Liang H, et al. Cartilage intermediate layer protein-1 alleviates pressure overload-induced cardiac fibrosis via interfering TGF-β1 signaling. *J Mol Cell Cardiol.* 2018;116:135–144.
46. Liu Y, Okesola BO, Pearce OM, Mata A, Heeschen C. Matrix Biology Europe–July 2018 Meeting Celebrating 50 years of Federation of European Connective Tissue Societies Meetings. *Int J Exp Path.* 2018;99:A1–A69.
47. Nguyen XX, Muhammad L, Nietert PJ, Feghali-Bostwick C. IGFBP-5 promotes fibrosis via increasing its own expression and that of other pro-fibrotic mediators. *Front Endocrinol*. 2018;9:601.
48. Yang Y, Wicks J, Haitchi HM, et al. Regulation of A disintegrin and metalloprotease-33 expression by transforming growth factor-β. *Am J Respir Cell Mol Biol*. 2012;46:633.
49. Gilger BC, Yang P, Salmon JH, Jaffe GJ, Allen JB. Expression of a chemokine by ciliary body epithelium in horses with naturally occurring recurrent uveitis and in cultured ciliary body epithelial cells. *Am J Vet Res*. 2002;63:942–947.